Indian Journal of Engineering & Materials Sciences
Vol. 27, April 2020, pp. 150-167

Tribological investigation of HVOF-spray Cr_3C_2-25NiCr and WC-10Co-4Cr coated turbine steel under varied slurry erosion conditions

Mithlesh Sharma[a], Deepak Kumar Goyal[b*] & Gagandeep Kaushal[c]

[a]Mechanical Engineering Department, I. K. Gujral Punjab Technical University, Kapurthala 144603, India

[b]Mechanical Engineering Department, I. K. Gujral Punjab Technical University, Main Campus, Kapurthala 144603, India

[c]Mechanical Engineering Department, Yadavindra College of Engineering, Punjabi University Guru Kashi Campus, Talwandisabo, Bhatinda 151302, India

Received:04 April 2018 ; Accepted:05 December 2019

In this work, high velocity oxy fuel (HVOF) method based spray coatings namely Cr_3C_2-25NiCr and WC-10Co-4Cr have been deposited on AISI304 turbine steels. An attempt has been made to analyze the coatings under accelerated slurry erosion conditions by employing a laboratory-developed slurry erosion testing set-up. The testing has been performed under varied conditions of slurry concentration, impact velocity and impact angle using the Taguchi approach. The microstructure of coating powder, erodent particles and deposited coatings have been studied using a scanning electron microscope (SEM) analysis. Erosion tests indicated that HVOF-spray Cr_3C_2-25NiCr and WC-10Co-4Cr coatings have been deposited on AISI304 steel exhibited significant improvements in the erosion resistance of AISI304 steel. The possible reason for such behaviour could be higher microhardness of HVOF-spray coatings in comparison with AISI304 bare steel. From SEM images of the samples taken prior and post slurry erosion tests, it has been observed that Cr_3C_2-25NiCr coating exhibited mixed (ductile and brittle) behaviour, though the WC-10Co-4Cr coating mostly demonstrated ductile behavior under conditions for erosion from the slurry. Apart from that, an attempt has been made to develop a functional equation based on the regression approach which could be employed to assess the erosion wear rate under a set of conditions. The predicted erosion wear results under varied conditions are in close relationship to experimental values.

Keywords: Hydro turbine, Wear, Slurry erosion, Thermal spray coatings

1 Introduction

In the contemporary industrial era, the demand for energy, particularly electricity is amplifying at an alarming rate[1]. Hydropower being a renewable source of energy has captivated the attention of researchers worldwide to fulfill the demand for energy requirement[2-5]. With increasing dependency on hydropower, more obligations have been laid on hydroelectric power stations which have culminated in the extensive usage of hydropower resources[6].

To cater to the demand, hydroelectric power plants are running under unfavourable conditions such as high silt content[7-8]. High silt content in the water leads to extensive material removal from various components of hydraulic machinery[8-9]. In particular, various components associated with hydro machinery such as turbine blades, labyrinth seals and guide vanes are on the extent of maximum damage by abrasive particles[1-2]. Wear of turbine components primarily occurs due to abrasion, which chiefly depends upon the mechanical and tribological properties of the target material and mechanical properties of solid particles carried by the fluid[6]. The erosive wear rate of the target surface depends upon the erodent's impact velocity and the angle with which these particles strike the target surface[8-9].

After reviewing the literature, it has been grasped that erosive wear is a function of several parameters such as the morphology of the erodent particles, hardness ratio between target surface to erodent's, slurry concentration and impact velocity of particles. In the majority of cases, it is minimized by regulating the above-referred parameters or by controlling the impact energy of the erodent particle[7-16].

The components of hydro-turbine are made up of stainless steel due to its exceptional properties such as high corrosion and erosion resistance[8-9, 12-13]. However, under severe operating conditions, it also suffers from excessive material loss due to erosive wear. Previous investigations reported that under such extreme conditions, thermal sprayed coatings played a

*Corresponding author (E-mail: erdeepakgoyal81@gmail.com)

key role in enhancing the working life of hydro-turbine materials[6-9, 17-20].

Performance of thermal spray coatings depends upon various factors such as surface preparation before coating, spray parameters, chemical and mechanical properties of powder to be deposited[17-23]. In the thermal spray coating process, the powder particles are heated and melted using chemical or electrical energy which further accelerates towards the substrate surface and gets deposited on it[24]. Among the various thermal spray coatings, HVOF-spray coating is used extensively due to remarkable features associated with its flames such as higher velocity, lower temperature and lesser dwell time, which resulted in a closely packed coating with good bond strength, higher hardness, lesser decarburization, lower porosity and oxide content[25-30.]

This study provides useful insights into the tribological behaviour of HVOF-spray Cr_3C_2-25NiCr and WC-10Co-4Cr coatings deposited on AISI304 turbine steel. So far, limited information about the possibilities of such material combinations has been reported in the open literature. To further enrich the study, the influence of erodent particles operating parameters such as impact angle, slurry concentration and impact velocity on the slurry erosion behaviour of uncoated and HVOF-spray coated AISI304 steel was analyzed. Furthermore, relative performances of the said material under different operating conditions were compared in terms of their composition and microstructure.

2 Experimental Procedure

2.1 Base Material

In the present study, Maneri Bhali stage-1, hydropower project, which is situated at Uttarkashi, Uttarakhand, India on the Bhagirathi river has been chosen for the case study. An eroded blade section of Francis turbine was cut by using an arc cutting technique and spectroscopic analysis (Spectromax, Indiana Lab, Mohali, India) of the same was carried out by using the arc spark Optical Emission Spectroscopy (OES). Results revealed that the components of Francis turbines were made up of AISI304 steel and therefore AISI304 steel was taken as a substrate material for the present study. Substrate material AISI304 steel was obtained from Ludhiana Steels, Punjab, which is a renowned company in the production and supply of such hydro machinery components. The chemical composition of the base material used in the present study is shown in Table 1. Further, it was observed that the mass density of steel was 7.8 g/cc. Microhardness of AISI304 steel was obtained by using Vickers microhardness tester (SHV-1000, SLIET, Longowal, India). For calculating microhardness value, the mean of ten microhardness readings was taken on the sample which helped out in reducing the probability of error. The specimens of the square section with size 40 mm and thickness 8 mm were prepared for slurry erosion testing.

2.2 Coating Deposition

In this study, commercially available Cr_3C_2-25NiCr and WC-10Co-4Cr coating powders were investigated for knowing their slurry erosion resistance under varied slurry erosion conditions. A detailed description of the same is provided in Table 2. The coating powders were deposited on AISI304 steel samples by employing a commercial HVOF thermal spray system (Hipojet 2700) facility available at M/S Metalizing Equipment Pvt. Ltd., Jodhpur, India. Conditions under which coating was carried out are presented in Table 3. For uniform solidification of the coatings, a compressed air jet was blown over the specimens during and post spraying process. Pre-deposition, sample surface treatment was carried out using Al_2O_3 as a grit particle to remove the oxide layer from the surface of the sample, which assists in attaining good coating adhesion by increasing the surface roughness over the sample.

2.3 Slurry

Silt particles used in the present study were taken from Maneri Bhali stage-1, hydropower project,

Table 1 — Chemical composition of AISI304 steel.

Grade	C_{max} (%)	Mn (%)	P (%)	Cr (%)	Si (%)	S (%)	Ni (%)	Fe (%)
AISI 304 steel	0.02	1.85	0.40	18	0.475	0.0302	8	Balance

Table 2 — Details of the coating powder used.

Powder	Make	Morphology	Particle shape	Particle size
Cr_3C_2-25NiCr	Hunter	Agglomerated sintered	Irregular/ Sub angular	–45 +15 µm
WC-10Co-4Cr	Woka 3552	Agglomerated sintered	Sub spherical	–45 +15 µm

Table 3 — Spray parameters used for HVOF-spray based coating deposition.

Oxygen flow rate	270 SLPM
Fuel (LPG) flow rate	60–65 SLPM
Airflow rate	650 SLPM
Spray distance	20 cm
Powder feed rate	28 gm/min
Oxygen pressure	10.0 kg/cm^2
Air pressure	5.5 kg/cm^2
Fuel pressure	6.5 kg/cm^2

Uttarkashi, Uttarakhand, India. Silt collected from the tail race of the hydropower plant was initially wet. To identify the presence of various particle sizes available in the silt, silt was placed under the sunbath and post drying, sieve analysis of the same was carried out. To study the morphological details of the erodent particle available in the silt, it was analyzed using the SEM facility. The SEM image of the erodent particle is shown in Fig. 1, which shows that particles comprised of irregular shapes with angular or semi-angular particles. To attain the average particle size of slurry as 155 µm, silt particles with varied size distribution were mixed in pre-determined quantity as reported by Singh *et al*.[31]. To determine the constituents element present in the silt particles, Energy Dispersive Spectroscopy (EDS) analysis was carried out which is shown in Fig. 2. EDS analysis revealed that silt particles comprised a mixture of silica particles, magnesium, aluminium and ferrous as a major constituent. To maintain the slurry concentration of varied ranges such as 10000 ppm, 20000 ppm and 30000 ppm, a pre-determined volume of water was mixed with the silt particles.

2.4 Characterization

To analyze the surface morphology, effects of coating on microstructure and mechanism resulted in degradation of surface, pre and post experimentation characterization of the coated and uncoated samples were carried out using SEM analysis. Optical microscope and image analyzer were used to measure the porosity of the coated samples (QSMIAS-40, SLIET, Longowal, India). It uses Envision 3.0 series software. Surface irregularities over the uncoated and coated samples were evaluated using a surface roughness tester (Surftest Sj301, Mitutoyo, IET Bhaddal, Ropar, India). The cross-sectional microhardness of the uncoated and coated steel was measured using a digital Vickers microhardness tester (SLIET, Longowal, India) at a load of 2.94 N with a dwell time of 15 seconds.

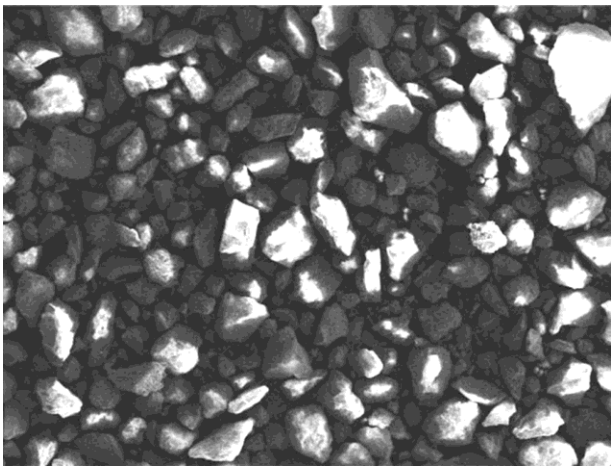

Fig. 1 — SEM image of slurry particles.

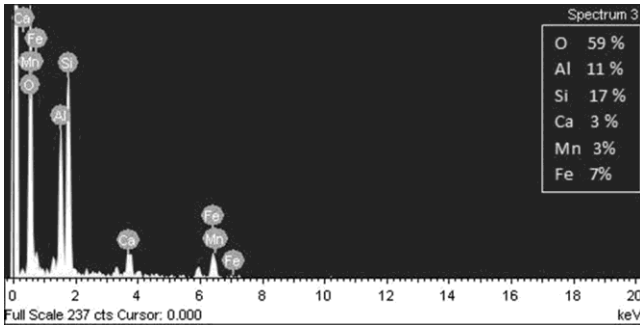

Fig. 2 — EDS analysis of slurry particle.

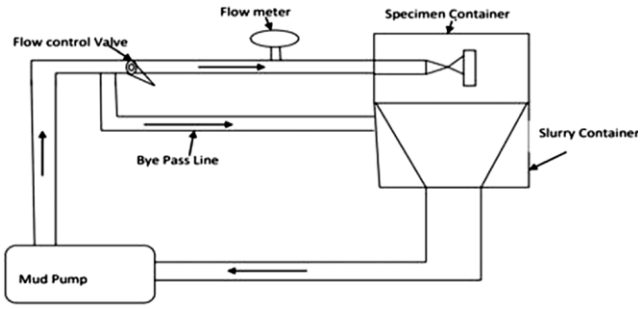

Fig. 3 — Schematic view of slurry erosion impact test rig.

2.5 Slurry Erosion Testing

The erosive behaviour of uncoated and coated samples was tested on laboratory-developed slurry erosion testing setup (IET Bhaddal, Ropar, India) as shown in Fig. 3. The setup consists of a mud pump, flow meter, valves, conical tank, specimen container and nozzle. Electric motor (5hp, 1400 rpm) drives the mud pump which generates high pressure (13.5 bar) and discharge rate (240 L/min). The slurry used for testing was recirculated and changed after 4 hours of testing. The slurry was placed in a tank having a rectangular shape (500 mm × 350 mm) at the top and further using a length of 1000 mm converged into a

square shape (side 80 mm) at the bottom. The flow rate of slurry flowing in the setup was regulated by using the main valve and bypass pipeline provided in-between the delivery side pipeline and nozzle. Due to the mechanical action of the pump, the slurry temperature rises to a certain level and further maintained constant by using bags filled with wet sand around the pipes. To restrict any workpiece from falling into the tank, the screened mesh was provided below the specimen container. Experiments were carried out on a range of parameters given in Table 4, with a particle size of 155 µm respectively. The time taken to conduct the slurry erosion test is 120 minutes per sample. The samples were cleaned thoroughly using acetone prior and post to erosion testing so that no impurities are left within the samples.

Mass loss was determined by conducting measurements on weight balance with an accuracy of 0.001 gram prior and post erosion testing. The mass loss for determining the erosion rate was calculated using the given below formula:

$$\text{Mass loss (mg/cm}^2) = (W_i - W_f) / A \quad \ldots (1)$$

where, W_i and W_f are the initial mass and final mass of each specimen pre and post 120 minutes of erosion testing expressed in mg, whereas A is the surface area expressed in cm^2.

2.6 Design of Experiments

The Taguchi L_9 orthogonal array approach was used to design the experiments and to analyze the individual operating parameter effect on the slurry erosion behaviour of tested material. The experimental conditions used for conducting slurry erosion tests are shown in Table 4. Further, for data analysis and the Design of Experiment (DOE), Minitab 17V software was employed. The analysis was done by considering the smaller the better approach. The S/N ratio for this function is determined by:

$$\eta = -10\log_{10}\left(\frac{1}{n}\sum_{i=1}^{n} y_i^2\right) \quad \ldots (2)$$

Table 4 — Parameters and their level for slurry erosion testing.

Parameter	Slurry concentration (ppm)	Impact velocity (m/s)	Impact angle (°)
Level 1	10000 (1% by mass)	25	30
Level 2	20000 (2% by mass)	50	60
Level 3	30000 (3% by mass)	75	90

Where η is signal to noise ratio, n is the number of observations, y is performance characteristics and i is the value of performance characteristics.

2.7 Experimental Conditions

Various investigators had tried to analyze the influence of operating parameters i.e. velocity, particle size and slurry concentration, on slurry erosion behaviour of target surface[7-8, 15–18]. The findings of these studies suggested that the erosion rate was significantly affected due to variation in these parameters. Gupta *et al.*[17] from experimental work derived a relationship for prediction of erosion rate:

$$E_r = KV^a d^b C^c \quad \ldots (3)$$

Where E_r is erosion rate, V is impact velocity, d is slurry particle size, C is slurry concentration, K, a, b and c are constants, the values of which are determined by the properties of erodent and target material. In this work, the effects of three parameters with three different levels were taken as shown in Table 4. These conditions were used to analyze the erosion behaviour of uncoated and HVOF-spray coated samples. The DOE was carried out according to Table 5 and the erosion rate results with different run conditions are also shown in Table 5.

3 Characterization

3.1 Morphology of Feedstock Powders

To analyze the morphological details of the feedstock powders used in this study, the SEM analysis using the SEM facility (JEOL JSM-6610LV) was carried out. From the SEM images of the coating powders, as shown in Fig. 4 and Fig. 5, it is depicted that these powder particles exhibited spherical and orthorhombic shape. Further, it has been observed that Cr_3C_2–25NiCr powder particles have a spongy structure with sub-micron particles. However, WC-10Co-4Cr powder particles exhibited mixed morphology with most of the particles having a nearly spherical shape and few particles having approximately semi-spherical structure. Furthermore, SEM images are shown in Fig. 4 and Fig. 5, reveals that the average size of WC-10Co-4Cr powder particles was smaller in comparison with the average size of Cr_3C_2–25NiCr powder particles. It has also been observed that Ni particles comprised of a round morphology, whereas tungsten carbide particles seemed to be formed by the agglomeration of several smaller particles in combination[3]. It was noticed that

Table 5 — Design of experiment using Taguchi L_9 orthogonal array and mass loss based on experimental conditions.

Experiment No.	Slurry Concentration (ppm)	Impact Angle (°)	Velocity (m/s)	Mass loss, AISI 304 Steel (mg/cm^2)	Mass loss, Cr_3C_2-25NiCr (mg/cm^2)	Mass loss, WC-10Co-4Cr (mg/cm^2)
1	10000	30	25	6.87	5.06	4.50
2	10000	60	50	9.12	5.31	5.93
3	10000	90	75	13.12	6.37	5.93
4	20000	30	50	11.65	5.31	5.62
5	20000	60	75	12.43	6.75	6.18
6	20000	90	25	8.75	5.31	5.37
7	30000	30	75	12.18	6.43	6.12
8	30000	60	25	12.81	6.25	5.75
9	30000	90	50	11.87	6.68	6.37

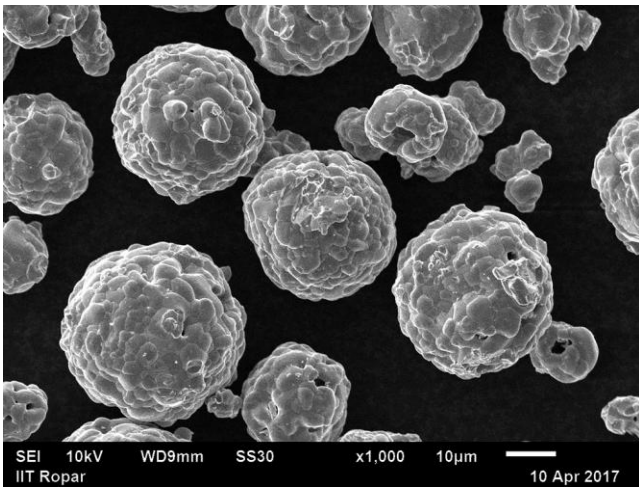

Fig. 4 — SEM image of Cr_2C_3-25NiCr feedstock powder.

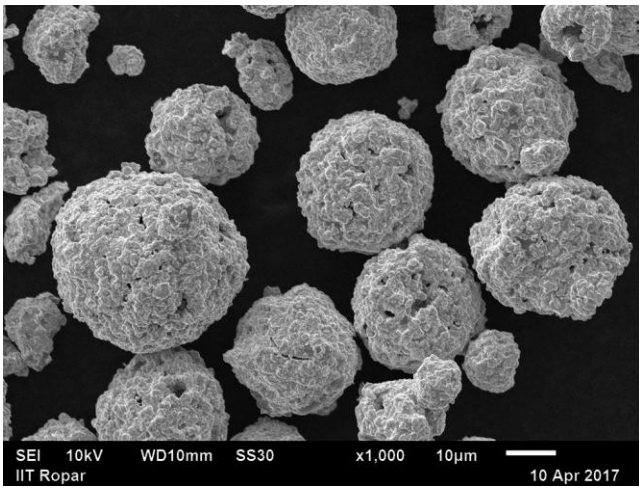

Fig. 5 — SEM image of WC-10Co-4Cr feedstock powder.

feedstock powder comprised of particles sized between 5 to 45 µm diameters. The previous investigation related to feedstock powder reported that particle size of feedstock powder significantly affects the deposition efficiency which results in lesser material loss and improved quality of the coating[18].

3.2 Morphology of Alumina Grit Particles

Prior to HVOF-spray coating deposition, samples were shot blasted with the help of alumina oxide grit particles, the morphology of the same has been shown in Fig. 6. It was observed that alumina grit particle comprised of sub-angular morphology. To identify the constituents of these grit particles, EDS analysis was carried out. It can be depicted that that grit particle comprises alumina particles, sand particles and oxides as shown in Fig. 7. These grit particles are propelled by the compressed air towards the sample surface. The oxide layers deposited on the specimen surface are removed on the impact of the grit particles and this also enhanced the surface roughness, which led to the improvement in coating deposition efficiency[7-8].

3.3 XRD Analysis

To analyze the various phase available in powder and as-sprayed coating, XRD analysis was performed using an x-ray diffractometer with copper as a target. XRD images of Cr_3C_2-25NiCr powder and as-sprayed Cr_3C_2-25NiCr coating are shown in Fig. 8(a) and Fig. 8(b) respectively. The XRD image as shown in Fig. 8(b), depicts that the solid solution phase was present in the coating. The formation of a metastable phase of Cr_7C_3 can also be observed from the XRD image, which may be due to the reaction of Cr_3C_2 with NiCr during the coating deposition process. The high temperature generated during the deposition of the coating by the HVOF-spray process results in the non-existence of the oxide phase.

Similarly, Fig. 9(a) and Fig. 9(b), presents the XRD images for WC-10Co-4Cr under both powder and as-sprayed conditions. It has been depicted that the

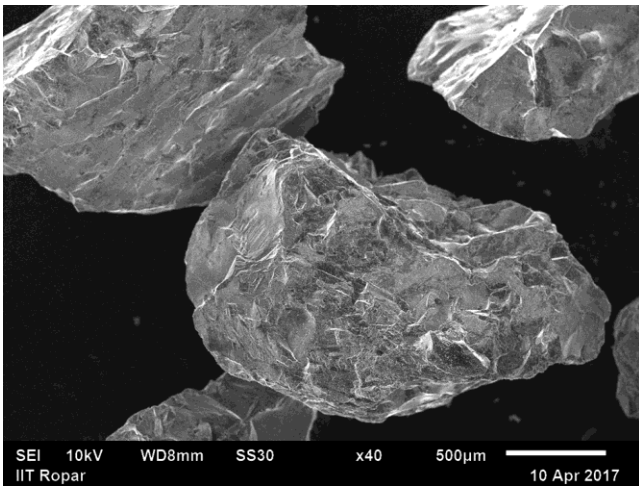

Fig. 6 — SEM image of alumina grit particles used for shot blasting.

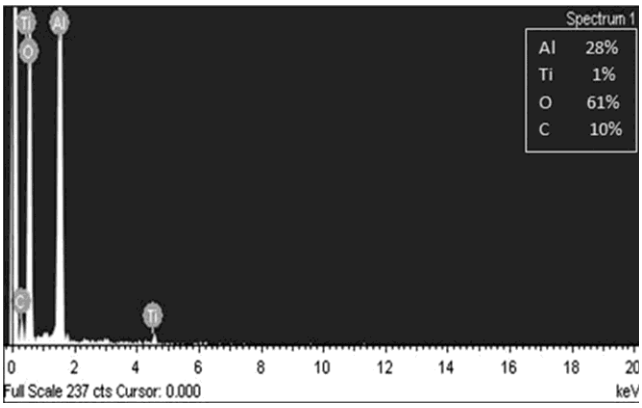

Fig. 7 — EDS analysis of alumina grit particles.

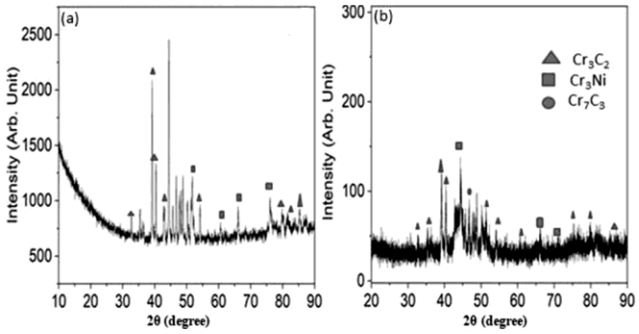

Fig. 8 — XRD micrograph of Cr_3C_2-25NiCr (a) Powder and (b) HVOF coating.

phases which were available post coating were not present in the powder diffractograph. In the as-sprayed coating, phases such as WC, W_2C,W and Co-based amorphous/nanocrystalline binder phases are commonly present, along with two other phases such as WC, Cr_2O_3CoO and W_2C. Previous investigations of the various researchers found that decarburization

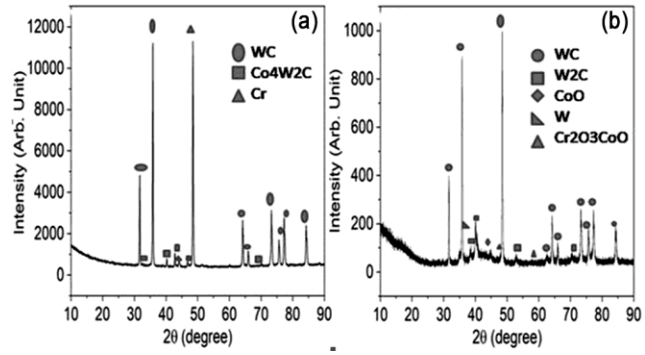

Fig. 9 — XRD micrograph of WC-10Co-4Cr (a) Powder and (b) HVOF coating.

of WC has a significant effect on tribological and mechanical properties[10-13]. According to them, lesser decarburization results in the higher hardness of the coated surface.

3.4 Microstructure

The microstructure of HVOF-spray Cr_3C_2-25NiCr and WC-10Co-4Cr coatings deposited on AISI304 steel was studied using the SEM facility. SEM images of as-sprayed Cr_3C_2-25NiCr and WC-10Co-4Cr coatings deposited on AISI304 steel are shown in Fig. 10 and Fig. 11 respectively. The SEM images revealed that the HVOF-sprayed coatings had distinctive melting degrees of thermal spray resulting in different types of surface morphology on the coated surface. SEM images further indicated the presence of a splat-like cross-sectional microstructure, a distinctive observation of the thermal spray coatings. The coated surface has shown interlocked molten splats with few unmelted particles fixed at some locations with uniform microstructure, From the SEM images, it appears that there is the presence of microscopic voids on the coated surface of the samples.

3.5 Microhardness, Apparent Porosity and Surface Roughness

To interpret the relationship between mechanical properties and slurry erosion behaviour of uncoated and HVOF-spray coated steel various dimensions such as microhardness, surface roughness (R_a) and apparent porosity were investigated. Results obtained from uncoated and HVOF-spray coated steels are given in Table 6. It was calculated that the microhardness value of AISI304 steel was varied between 220-260 $HV_{2.94N}$ with an average value of 240 $HV_{2.94N}$. Similarly for HVOF-spray Cr_3C_2-25NiCr and WC-10Co-4Cr coatings deposited on AISI304 steel, the hardness value obtained was found to be fluctuating between 900-1050 $HV_{2.94N}$ and 1000-1200 $HV_{2.94N}$.

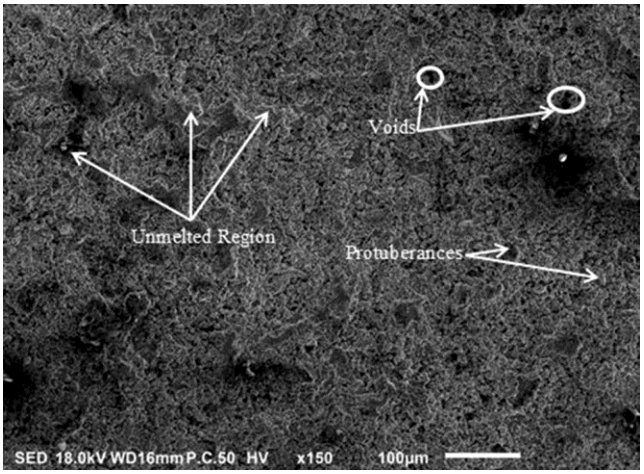

Fig. 10 — SEM image of HVOF-spray Cr_3C_2-25NiCr coated steel.

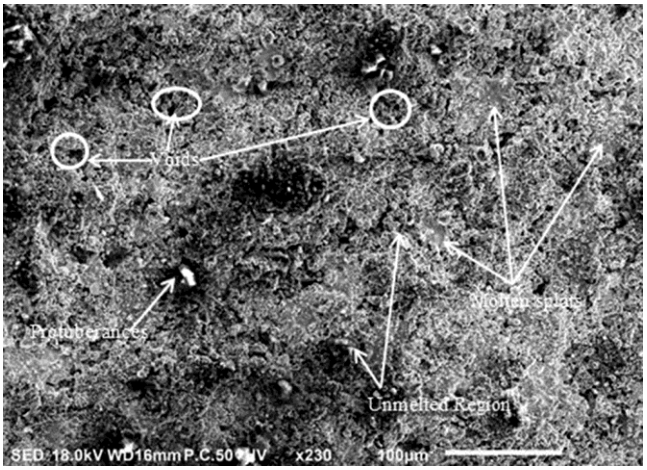

Fig. 11 — SEM image of HVOF-spray WC-10Co-4Cr coated steel.

Table 6 — Microhardness, apparent porosity and Surface roughness Ra values of investigated specimens.

Materials	Avg. Microhardness ($HV_{2.94N}$)	Apparent Porosity (%)	Roughness Ra (µm)
Uncoated AISI304 steel	237	-	1.56
Cr_3C_2–25NiCr coated steel	960	1.8	3.16
WC-10Co-4Cr coated steel	1129	1.6	3.78

The prominent reason for variations in the microhardness of the coating is due to the anisotropic nature of the thermal sprayed coatings which resulted from the presence of pores, voids, splat, splat boundaries and melted or unmelted particles as observed in the SEM images. It was observed that both the HVOF-spray coated surfaces have shown a significant increase in the microhardness values when compared with the bare steel surface. Furthermore, it was observed that HVOF-spray WC-10Co-4Cr coating has a higher hardness relative to HVOF-spray Cr_3C_2-25NiCr coating.

Apparent porosity results were obtained by using an optical microscope. It was observed that the apparent porosity of HVOF-spray coated samples was found to be less than 2%, which is in agreement with the findings of previously stated literature for HVOF-sprayed coatings. To assess the roughness value of the coated surface, sample analysis was carried out with a surface roughness tester. The higher surface roughness of the as-sprayed sample was found as compared to uncoated AISI304 steel samples.

4 Results and Discussion

4.1 Slurry Erosion

Using conditions mentioned in Table 5, slurry erosion behaviour of uncoated AISI304 steel, HVOF-spray Cr_3C_2-25NiCr and WC-10Co-4Cr coated steel was evaluated. Fig. 12 shows cumulative erosion loss observed under the various test conditions by the uncoated and HVOF-spray coated steel.

The mass loss per unit surface area results obtained from the investigated coatings and steel indicated that the HVOF-spray Cr_3C_2-25NiCr and WC-10Co-4Cr coatings showed a lesser mass loss in comparison with uncoated AISI304 steel in all test conditions. Further, it can be noted that the HVOF-spray WC-10Co-4Cr coating demonstrated better erosion resistance compared to Cr_3C_2-25NiCr coating, possible reason for such behaviour could be the better hardness of the WC-10Co-4Cr coating compared to Cr_3C_2-25NiCr coating. A similar reason could be suggested for higher erosion resistance of HVOF-spray coatings in contrast with uncoated steel.

Apart from that, it was also observed that during early cycles, the higher erosion rate of the coated specimen took place when compared to the later cycles. Such behaviour can be attributed to the presence of valleys and micro peaks on the surface of specimens. Such microstructures appear to be quickly sheared by the impacting particles resulting in higher erosion levels during the initial phase.[27]. However, overtime, the surface of HVOF-spray coated steel started to become smooth. As a result, the erosion rate variation comes under a narrow range steadily. Fig. 12(a-i) shows that erosion rate is affected by

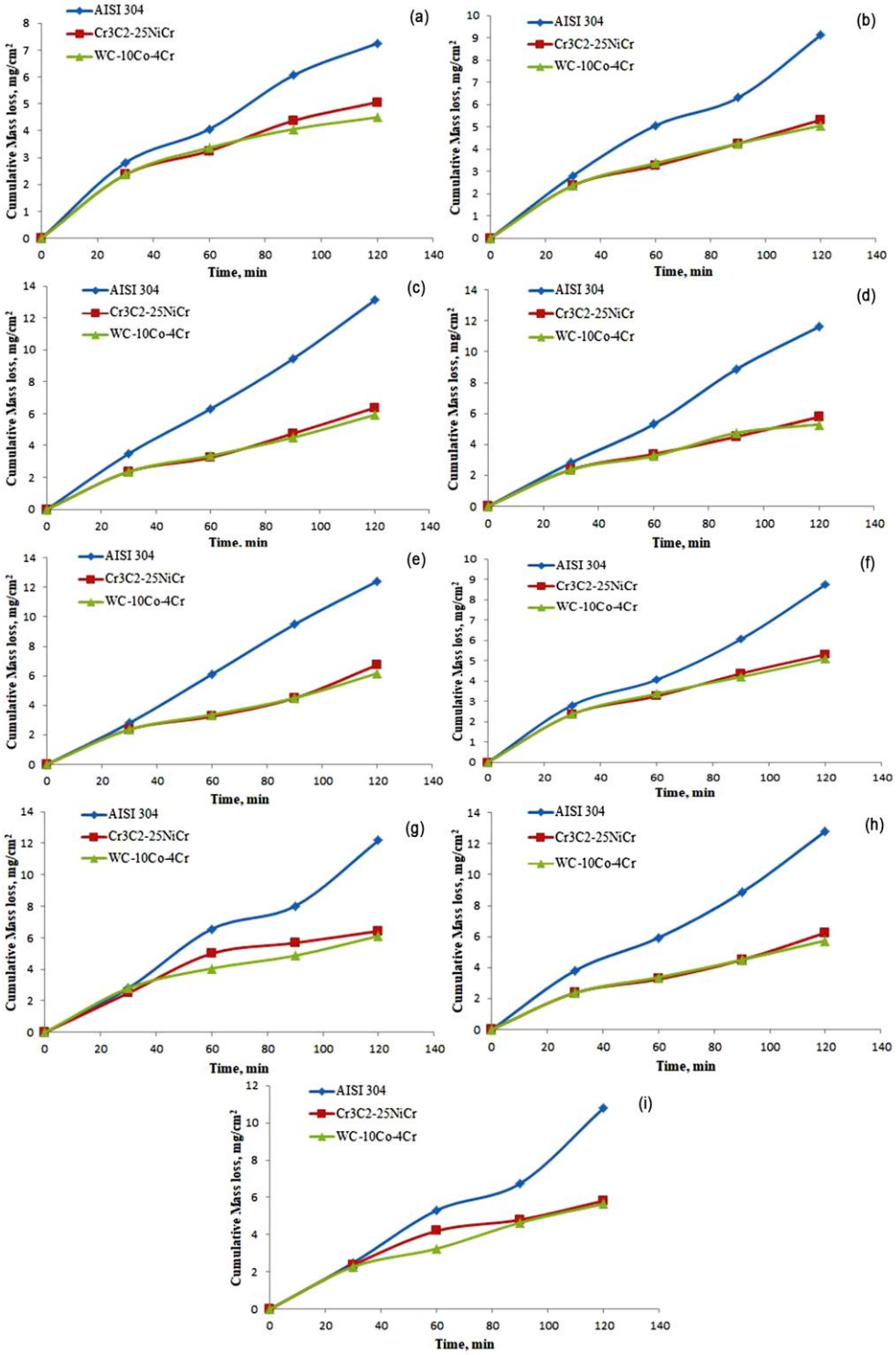

Fig. 12 — Cumulative erosion curves for uncoated and HVOF-spray Cr_3C_2-25NiCr and WC-10Co-4Cr coated steel specimens at (a) 25 m/s with slurry concentration of 10,000 ppm at impact angle 30°, (b) 50 m/s with slurry concentration of 10,000 ppm at impact angle 60°, (c) 75 m/s with slurry concentration of 10,000 ppm at impact angle 90°, (d) 50 m/s with slurry concentration of 20,000 ppm at impact angle 30°, (e) 75 m/s with slurry concentration of 20,000 ppm at impact angle 60°, (f) 25 m/s with slurry concentration of 20,000 ppm at impact angle90°, (g) 75 m/s with slurry concentration of 30,000 ppm at impact angle 30°, (h) 25 m/s with slurry concentration of 30,000 ppm at impact angle 60° and (i) 50 m/s with slurry concentration of 30,000 ppm at impact angle 90°.

different parameters such as impact velocity, impact angle and slurry concentration concerning the range of experimental conditions for uncoated, HVOF-spray Cr_3C_2-25NiCr and WC-10Co-4Cr coated steel.

4.1.1 Effect of impact velocity

Given the fact, that erosive wear occurred given the relative physical contact of the slurry particles with the target surface, it is highly anticipated that with further increase in velocity of striking particles, more particles will interact with the target surface which resulted into a higher amount of erosion from the surface of the material. Previous studies related to the velocity effect on erosion rate have verified this fact[24]. It was also revealed that higher erosion loss occurred with an increase in velocity since higher velocity leads to a significant increase in kinetic energy which is available for impact on the target surface.

In general, the erosion rate E, in erosion process is directly proportional as a power function of velocity V, i.e. $E \alpha V^n$ where n is velocity exponent and generally lies between 0.8 and 1.2[7-8]. Its value shows dependence on material removal mechanism, erodent particles morphological properties etc. The effect of impact velocity on the erosion rate of uncoated steel, HVOF-spray Cr_3C_2-25NiCr and WC-10Co-4Cr coated steel is presented in Fig. 13. It was found that maximum erosion loss for all ranges of velocity has taken place in uncoated AISI304 steel followed by HVOF-spray Cr_3C_2-25NiCr and WC-10Co-4Cr coated steel.

The findings of the study revealed an interesting fact, even at the low velocity, the consequences of impact angle were substantially insignificant in comparison with higher velocities. The effect of impact angle progressively increases with the increase in slurry velocity. It is associated with the fact that at low velocity, low kinetic energy is generated and this lesser energy leads to a lesser number of abrasive particles which will attain sufficient energy to cause plastic deformation on the target surface. With the further increase in velocity more particles acquired the critical energy which is required to cause material deformation and removal.

Besides, the present work also suggested that at lower velocity, the majority of the impact is elastic which doesn't cause much significant erosion of the samples. It is further observed that erosion at a lower impact angle is higher. The reasons depicted by various researchers[32] for such kind of behaviour in the case of ductile material is due to lesser energy

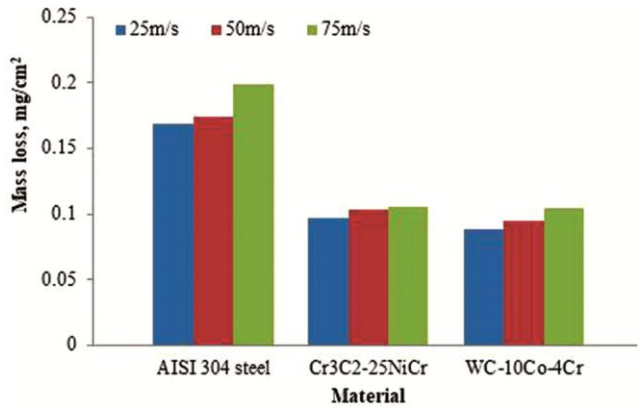

Fig. 13 — Effect of impact velocity on erosion rate of uncoated, HVOF-spray Cr_3C_2–25NiCr and WC-10C0-4Cr coated steel.

requirement for removal of material and higher surface area in contact at lower impact angle. This results in the action of two degradation mechanisms such as ploughing and cutting. At a high impact angle, the target surface deforms significantly even before the material is removed from the target surface. It suggests that erosion is almost independent of particle velocity at a lower impact angle. However, the reliance of erosion on the particle velocity is noticeable at a high impact angle.

Also, the Kinetic energy of the particles amplifies with the rise in the velocity of the slurry. In the meantime, slurry particles striking the target surfaces increases simultaneously. From Fig. 13, it has been observed that the impact velocity has a significant impact on the erosion rate. Mass loss due to erosion of the uncoated and coated material increases severely with a rise in the velocity of slurry. The results of the slurry erosion tests are following the findings of Goyal *et al.*[8-9]. It was proposed that the erosion rate is directly proportional to impact velocity. It was further exhibited from Fig. 13, that with an increase in velocity, proportionately results are not indicated in the erosion rate. It might be based on fact that actual erodent particle interaction with the target surface takes place at a much lesser value of velocity than the impact velocity emanated from the nozzle in the slurry erosion tests due to particle rebounding and fluid dynamic effects[8-9,21].

4.1.2 *Effect of impact angle*

The influence of impact angle on erosion rate of uncoated AISI304 steel, HVOF-spray Cr_3C_2–25NiCr and WC-10Co-4Cr coated steel is shown in Fig. 14. The figure indicates that the erosion rate for uncoated steel increases with the decrease in impact angle of

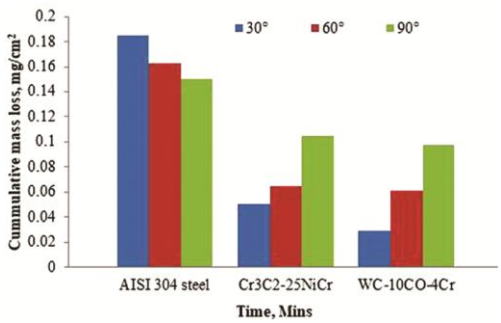

Fig. 14 — Effect of impingement angle on erosion rate of uncoated, HVOF-spray Cr_3C_2–25NiCr and WC-10Co-4Cr coated steel.

the slurry particle whereas in the case of HVOF-spray Cr_3C_2–25NiCr and WC-10Co-4Cr coatings opposite trend is observed.

Several phenomena were correlated as the reason for such a decrease in erosion rate. Firstly, it has been observed that at a low impact angle, the higher surface area of the substrate comes into contact with abrasive particles in comparison to a higher impact angle. Due to the slanting angle of abrasive particle, more elongated indent scratches are produced in comparison with a vertical indent that has been visualized in case of normal impact angles. This results in a higher value of scratch elongated into the direction of particle motion. Secondly, it is a well-known fact that the cutting action due to particle impingement at the oblique angle is more dominant than normal impact angles during slurry erosion. Thirdly, it has been observed that at a normal impact angle particles are rebounded back, which resulted in deflection of abrasive particles from their incoming path of impact, such phenomenon is not taking place at low impact angles i.e. 30°, which leads to a higher material loss. Fourthly, it was revealed that erodent particles get embedded into a matrix of the specimen at a high impact angle, the embedded particle itself acted as a reinforced particle which provides strength to the matrix against erosion.

Furthermore, embedded sand particles in the matrix of the specimen enhanced the mass and sluggish down the degradation of the surface by acting as a shielded layer over the target surface. It was observed that at a lower impact angle of erodent particles, metal removal takes place dominantly due to micro-cutting and ploughing mechanism while at higher impact angle the strain rate value is higher which leads to deformation of the uncoated steel into a plastic zone. It results in squeezing of the material inside the erosion marks without being completely removed.

Moreover, to further enrich the assessment regarding the impact angle on velocity, exponent n, was obtained from the erosion data presented in Table 5, which was curve fitted using the non-linear square fit method. The value of n found was 2.2, 1.2 and 1.1 respectively, which conform with the previous studies [25-26]. In the present work, it was observed that velocity exponent (n) reduces with the enhancement in impact angle. The possible reasons for such kind of behaviour at a high impact angle could be due to intrusion of more particles in the material matrix which acted as a barrier against erosion. This fact was verified with the help of SEM images. Embedded particles in the target matrix lead to a reduction in velocity exponent at a higher impact angle.

4.1.3 *Effect of slurry concentration*

The influence of slurry concentration on the slurry erosion behaviour of uncoated, HVOF-spray Cr_3C_2-25NiCr and WC-10Co-4Cr coated AISI304 steel is shown in Fig. 15. From the figure, it is clear that AISI304 steel with HVOF-spray coatings exhibited much higher erosion resistance in comparison with uncoated steel. It was observed that with the rise in slurry concentration, drastic increase noticed in the erosion rate of AISI304 steel whereas a slight increase observed in erosion rate of HVOF-spray coated AISI304. The HVOF-spray WC-10Co-4Cr coating provides much better erosion resistance than HVOF-spray Cr_3C_2-25NiCr coating with the rise in slurry concentration.

In general, it was a well-established fact that with the increase in slurry concentration higher number of solid particles entrained in the slurry for interaction with the target surface which resulted in a higher erosion rate. In the present study, a similar trend is observed up to a threshold value, once slurry erosion reaches this value, the erosion rate started to decline the erosion rate with a further increase in slurry concentration. The fact for such a decline in the erosion rate was suggested to be the screening effect[26] due to the availability of redundant sand particles in the slurry. The redundant sand particle available in the slurry causes a collision of the sand particles with each other and as a result of which effective interaction between slurry and the target surface decreases. This diverged redundant sand particles might be embedded in a matrix of the specimen or available on the surface which causes a further potential for reduction in the erosion process due to the formation of a barrier layer.

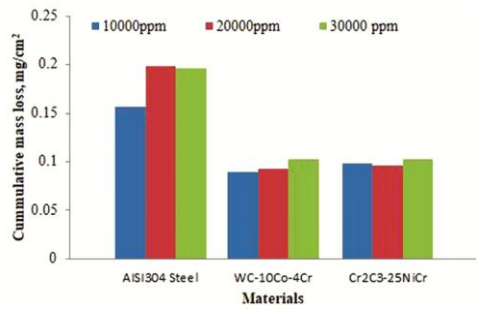

Fig. 15 — Effect of slurry concentration on erosion rate of uncoated, HVOF-spray Cr_3C_2–25NiCr and WC-10Co-4Cr coated steel.

4.2 Taguchi and Analysis of Variance (ANOVA)

In this work, the L_9 orthogonal array of Taguchi design of experiments approach is adopted for the exploration of obtained results as illustrated in Table 5. Higher mass loss was noticed in run number 5 (i.e. slurry concentration, 20000 ppm, impact velocity, 75m/s and impact angle of 60°) and minimum mass loss was observed in the run number 1 (i.e. slurry concentration, 10000 ppm, impact velocity, 25m/s and impact angle of 30°) for both uncoated and HVOF-sprayed coated AlSI304 steel.

4.2.1 Response plots

The effect of various factors on the slurry erosion behaviour of uncoated AISI304 steel, HVOF-spray Cr_3C_2-25NiCr and WC-10Co-4Cr coated steel was studied using response plots[26]. Fig. 16-18, illustrate the main effect plots of various parameters for uncoated and coated AISI304 steel as per the L_9 orthogonal array approach of the Taguchi design of experiment (DOE). It depicts that an increase in erodent particles, impact velocity and slurry concentration, increases the erosion rate drastically, while an increase in impact angle, increases the erosion rate up to a certain limit for both coated and uncoated steel. Once this point reaches a further increase in impact angle has not much influence on mass loss due to erosion.

4.2.2 Interaction plots

Interaction of various process parameters (slurry concentration, impact angle and impact velocity) for the slurry erosion results was plotted by using Minitab 17V software. From the interaction plot of investigated parameters, namely slurry concentration, impact angle and impact velocity on slurry erosion of uncoated, HVOF-spray Cr_3C_2-25NiCr and WC-10Co-4Cr coated AISI304 steel, are shown in Fig. 19, 20 and 21,respectively. From Fig. 19, which shows the

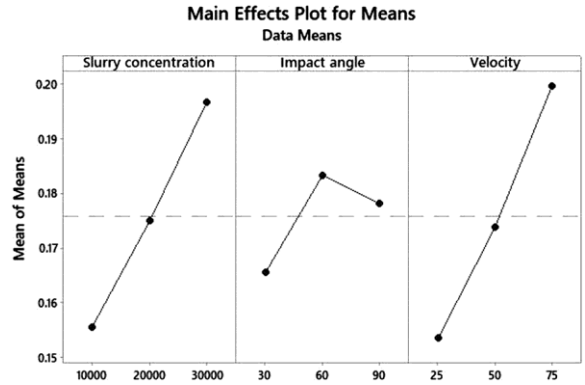

Fig. 16 — Main effect plots for AISI304 steel.

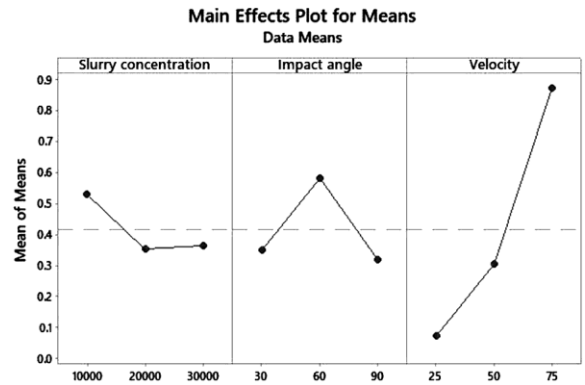

Fig. 17 — Main effect plots for HVOF-spray Cr_3C_2-25NiCr coated steel.

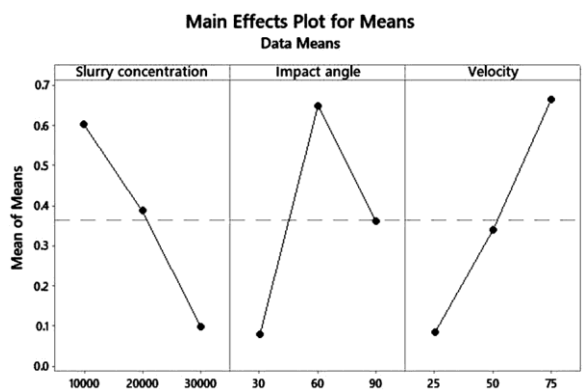

Fig. 18 — Main effect plots for HVOF-spray WC-10Co-4Cr coated steel.

interaction plot between various parameters for erosion loss in the case of AISI304, it is observed that the two lines in the plot are not parallel to each other which suggests that the interaction exists between impact angle and slurry concentration on slurry erosion of uncoated AISI304 steel. Since the angle of inclination is very small between the two lines thus it can conclude that interaction is not so severe. Also, it can conclude that the angle of the intersection of the

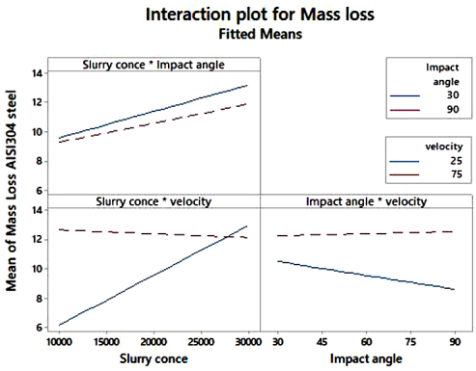

Fig. 19 — Interaction plot for AISI304 steel for various factors.

Fig. 20 — Interaction plot for HVOF-spray Cr_3C_2-25NiCr coated steel for various factors.

former is smaller than that of later. This suggests that comparatively stronger interaction exists between slurry concentration and impact velocity as compared to that of slurry concentration and impact angle. Furthermore, the angle of intersection between the two lines given in the plot is relatively larger, thus a greater interaction takes place between impact angle and impact velocity among all the discussed interactions.

Similarly, in the case of HVOF-spray Cr_3C_2-25NiCr coated steel as shown in Fig. 20, it is noted that the two lines in case of slurry concentration and impact angle are parallel to each other. It suggests that lesser interaction between these two parameters has taken place. Further, it was analyzed that two lines in the plot intersected at a higher angle between impact angle and impact velocity compared to the plot of slurry concentration and impact velocity, this suggests a stronger interaction in the case of the former one. Furthermore, it is noted that two lines in the plot intersect each other at a relatively larger angle, this

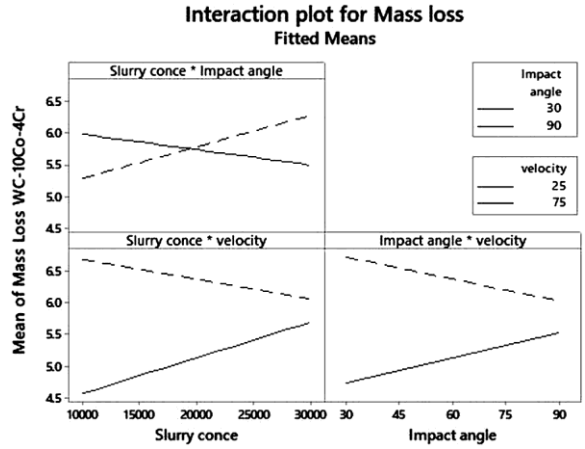

Fig. 21 — Interaction plot for HVOF-spray WC-10Co-4Cr coated steel for various factors.

suggests a severe interaction between impact angle and impact velocity.

Likewise, in the case of HVOF-spray WC-10Co-4Cr coated steel as shown in Fig. 21, it is noted that the two lines in the plots, slurry concentration and impact angle, intersected each other, hence it can be deduced that severe interaction among the two has taken place. Similarly, the intersecting angle between the two lines is lesser than the angle formed between the impact angle and impact velocity. Hence, it can be deduced that stronger interaction has taken place in case of impact angle and velocity in comparison with slurry concentration and impact velocity.

4.2.3 Analysis of variance (ANOVA)

The ANOVA analysis of obtained results was carried out to investigate the statistical significance of each factor and their contribution to the slurry erosion behaviour of uncoated and HVOF-spray coated steel. Table 7-9, reveals the ANOVA result for uncoated, HVOF-spray Cr_3C_2-25NiCr and WC-10Co-4Crcoated steel. The last column of the table represents the significance of each factor on the response variable. It indicates the influence of each factor considered in the present study on the slurry erosion behaviour of uncoated and coated steel.

To identify the significant parameters, effecting the erosion behaviour of uncoated and coated AISI304 steel, ANOVA analysis was performed. Table 7-9, shows the static ‘F’ values derived from ANOVA calculations as well as the percentage contributions in the slurry erosive behaviour of uncoated and coated steel. It is depicted that the velocity has a higher value of static ‘F’followed by slurry concentration and impact angle in case of uncoated AISI304 steel.

Table 7— ANOVA results of AISI304 steel.

Parameter	DF	Adj SS	Adj MS	F-Value	P-Value (%)
Slurry concentration	2	.002565	.001282	0.92	0.521
Impact angle	2	.000665	.000332	0.24	0.808
Velocity	2	.003713	.001856	1.33	0.429
Error	2	.002792	.001396		
Total	8	.009734			

Table 8 — ANOVA results of HVOF-spray Cr_3C_2-25NiCr coated steel.

Parameter	DF	Adj SS	Adj MS	F-Value	P-Value (%)
Slurry concentration	2	.000321	.000160	3.58	0.218
Impact angle	2	0.000134	.000067	1.49	0.401
Velocity	2	0.000403	.000201	4.50	0.182
Error	2	0.000090	.000045		
Total	8	0.000947			

Table 9 — ANOVA results of HVOF-spray WC-10Co-4Cr coated steel.

Parameter	DF	Adj SS	Adj MS	F-Value	P-Value (%)
Slurry concentration	2	0.000328	.000164	13.19	.070
Impact angle	2	.000088	.000044	3.54	.220
Velocity	2	.00295	.000147	11.85	.078
Error	2	.000025	.000012		
Total	8	.000736			

It also indicates that the impact velocity factor has a major impact on slurry erosion behaviour of uncoated AISI304 steel in comparison with other factors like slurry concentration and impact angle. In the case of HVOF-spray Cr_3C_2-25NiCr coated steel, it is observed that it followed the same trend as followed by uncoated steel, while in the case of HVOF-spray WC-10Co-4Cr coated steel the trend has changed. It has depicted that slurry concentration is the most dominating factor followed by impact velocity and impact angle.

The Regression equation for uncoated AISI304 steel, HVOF-spray Cr_3C_2-25NiCr and WC-10Co-4Cr coated steel was anticipated and based on these equations results were obtained. To validate these equations, a comparison was made with actual test results. It was observed that the obtained result was in closer agreements with the test results. Regression equations for tested materials are given below:

Mass loss of AISI304 Steel = 0.0761 + 0.000002*slurry concentration + 0.000211*impact angle + 0.000920*velocity

Mass loss of HVOF-spray Cr_3C_2-25NiCr coated AISI304 Steel = - 0.186 - 0.000008*slurry concentration - 0.00051*impact angle + 0.01600*velocity

Mass loss of HVOF-spray WC-10Co-4Cr coated AISI304 Steel = 0.004 - 0.000025*slurry concentration + 0.00472*impact angle + 0.01157*velocity

5 Examination of Erosion Mechanism

In an actual environment of the hydropower plant, the erodent particles along with the flowing water strike the turbine surface at different incident angles. Similarly, this work tried to create the slurry erosion conditions as available at a hydropower plant to investigate the effectiveness of the work carried out. Square shaped samples were placed in the chamber, slurry particles emanating from the nozzle, impact the sample surface to analyze its slurry erosion behaviour.The degradation mechanism which acted during slurry erosion conditions relies on the target surface properties and the incident angle of erodent particles[22].

The mechanical properties of the material, i.e. ductility and brittleness, leads to different erosive wear mechanisms. The ductile material resulted in the higher erosion rate at a smaller incidence angle i.e. 15º to 30º and at higher incidence angles the erosion rate gradually declines. At a lower incidence angle, direct cutting along with chip removal of material takes place from the target surface. It was noted that sometimes ploughing acted on a target surface which causes groove formation and resulted in the formation of lips or platelets. These lips or platelets were detached from the surface due to abrasive fatigue by subsequent impacts of slurry particles. However, a higher incidence angle, i.e. 90º, resulted in an indentation on the surface of the sample along with displacement of material outwards. Consequently, the formation of deep crater due to the inter-spallation of layers occurred. Besides that, repeated incidents of particles on the strained material resulted in the loss of material due to fracture or fatigue[28].

The brittle material resulted in higher erosion loss due to a larger impact angle i.e. 90° and reduces significantly with the lower value of impact angle.

At a higher impact angle, the impacting particles illustrated brittle fracture which resulted in the development of cracks in the outward and downward direction from the point of impact. In such cases, material eroded due to microchipping resulted in the ejection of small fragments from the target surface. Also, the impact of slurry particles onto the intersection of the crack network emanates material from the surface[24,26]. However, at a lower impact angle, initiation of crack does not occur. It results in erosion of material due to plastic deformation which symbolizes the occurrence of shear deformation mechanism[10]. In general, erosion on the surface of ductile materials took place due to the action of various mechanisms such as micro-cutting or plastic deformation, followed by cutting. Similarly, fatigue failure due to the transfer of energy by the repetitive impact of slurry particles causes degradation in the brittle materials[10].

SEM analysis using JEOL 6610LV was carried out to analyze the degradation mechanism which resulted in erosion loss over the target surface. Fig. 22(a-b) shows the AISI304 steel surface before erosion testing which shows the presence of microcracks, coarseness in the shape of pits, coincident cracks on the subsurface and fractured fragments. Slurry erosion testing has shown that the degree of erosion on the uncoated substrate is more severe than that of HVOF-spray coated specimens. Erosion damage was attributed due to the presence of the high rate of wear debris on the surface.

Post erosion test of the AISI304 steel sample as shown in Fig. 23(a-c), it was observed that degraded surface comprised of plastically deformed craters and cracked fragments. These findings suggest an erosion of material owing to micro-cutting action which results in the formation of cracks and damage caused by erodent particles due to abrasive action. This behaviour is attributed to the lower hardness of the substrate rather than corrosion on uncoated AISI304 steel. These observations are in line with the other researchers[8-9, 28].

In the case of surface degradation on AISI304 steel at 30°, cutting action of erodent particle resulted in pitting and ploughing action which caused the formation of tiny grooves in the degraded surface. Such grooves were further found to be lined with fractured fragments. High fragmentation and sliding action of slurry particles were attributed to such behaviour of the target surface. In the context of wear

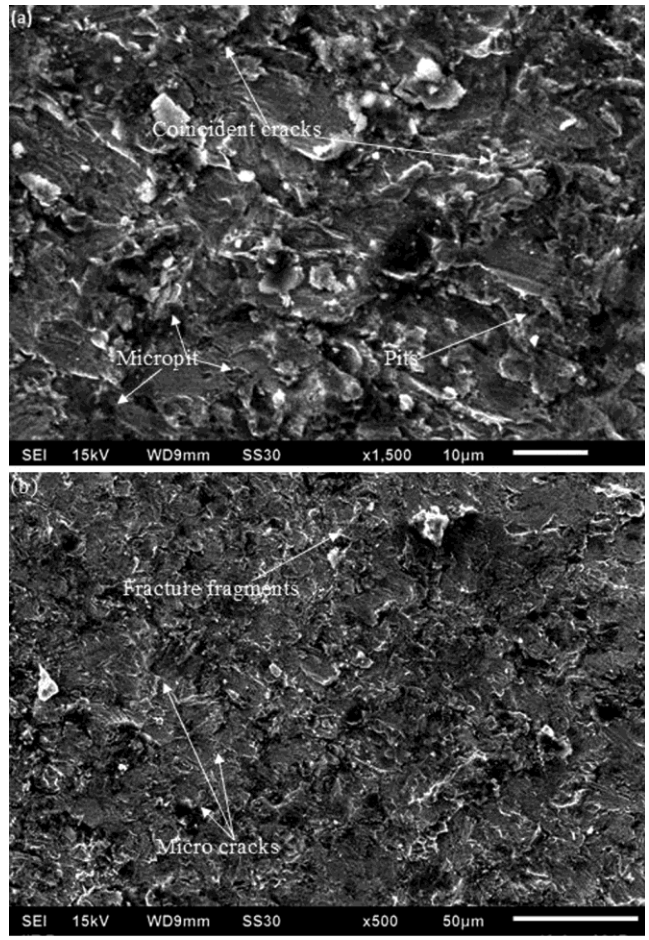

Fig. 22 — SEM images of uncoated AISI304 steel (a) SEM ×1500 and (b) SEM ×500.

damage at 60°, it was observed that the impact of slurry particles produces wear debris along with large fractured fragments that fill the grooves and micro-pit on the surface. Furthermore, some wear debris have been found to either flattened or smeared the target surface. Moreover, plastic deformation has also taken place on the surface due to the abrasive action of slurry particles.

Further, it was noticed that amongst the impact angles considered, maximum erosion occurred at a 60° impact angle. This indicates that the most effective cutting action by abrasive particles as shown in Fig. 23(b), prompted higher material removal from the target surface.

Similarly, Fig. 23(c) shows the degraded surface at a 90° impact angle. It was observed that there was a presence of deep craters on the substrate surface. It might be due to ploughing action carried by the erodent particles on the target surface which led to material removal. Moreover, degradation of the

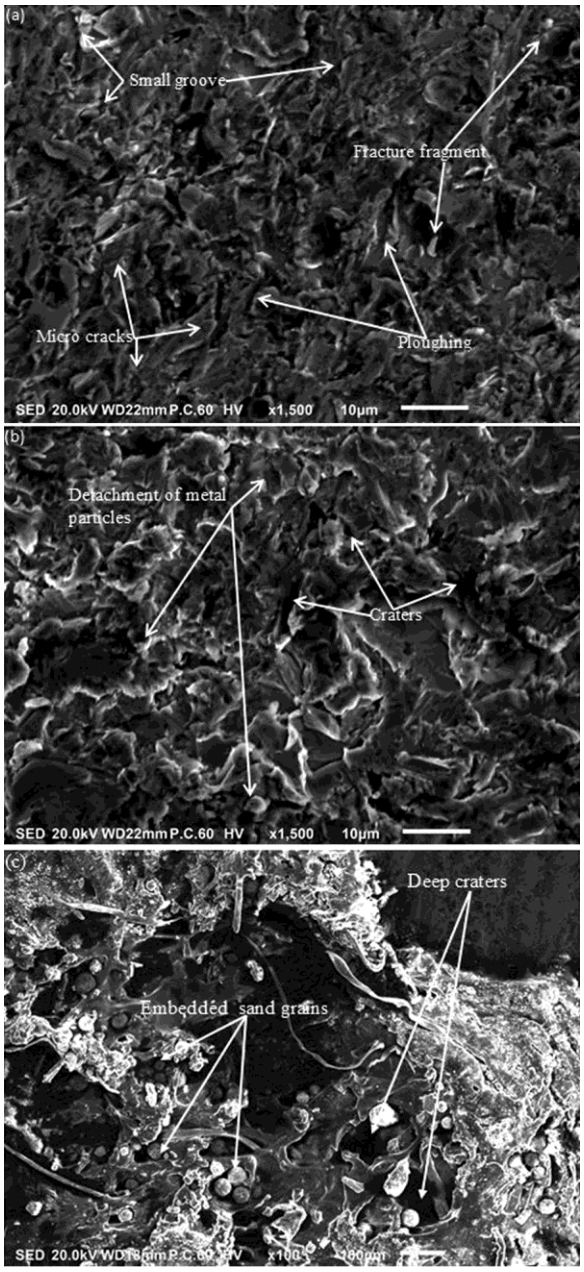

Fig. 23 — SEM images of AISI304 steel post 120 mins of erosion testing at various impact angle (a) 30°, (b) 60° and (c) 90°.

surface was depicted to be occurred by the platelet mechanism. These observations are in closer agreement with the findings of other researchers[21]. Furthermore, the impact of slurry particles on the target surface leads to the formation of a crater which further extruded to form raised micro crack. The subsequent impact of slurry particles on the target surface causes deformation of displaced material which results inside-movement of material followed by ductile splintering at the highly strained region. Repetitive impacts make the displaced material severely strained, ultimately results in detachment from the target surface by ductile fracture[8]. Similar findings have been observed from the SEM images. Moreover, the erosive rate is not higher at the 90° impact angle although the slurry particles possess enough energy to cut a chip from the surface. This may be due to the rebounding motion of the erosion particles which deviates the direction of the approaching particles and strikes them at different positions of the target surface.

The SEM image of HVOF-spray Cr_3C_2-25NiCr coating on AISI304 steel under various conditions of slurry erosion is shown in Fig. 24(a-c). It was depicted in Fig. 24(a) that under the slurry erosion conditions of impact velocity 25 m/s, impact angle 30° and slurry concentration of 10000 ppm, the degradation of the surface occurred as a result of micro-chipping at splat boundaries. As shown in the figure that the coating surface comprises of small and large carbide splats. The impact of erodent particle on these large carbide size particles leads to degradation of surface in a brittle manner which further extended to splat boundary.

As the slurry concentration and impact velocity are lower, the kinetic energy produced under such conditions being lower, neither plastic deformation nor ploughing was noticed in such conditions. At impact velocity 25 m/s, impact angle 60º and slurry concentration 30000 ppm, it can be seen from Fig. 24(b) that micro-cutting was found to be a degradation mechanism for erosion. Furthermore, localized chip formation has been observed owing to the brittle cracking of carbide particles.

The increase in kinetic energy resulted from higher impact velocity, i.e. 25 m/s to 75 m/s and higher impact angle of 90º, resulted in deeper penetration of the erodent particle as seen in Fig. 24(c). Further, some erodent particles were found embedded inside the material which might have resulted in a lesser erosion rate of the coated surface. Fig. 24(b) and 24(c) revealed that an increase in impact angle and impact velocity has a significant effect on the degradation mechanism. Erodent particles under such conditions result in the smoothening of the Cr_3C_2–25NiCr coating surface which resulted in significant changes in morphology. Furthermore, it has been observed that there is a presence of many voids on the coating surface, which arose due to the removal of unmelted particles. Some lip marks have been observed which

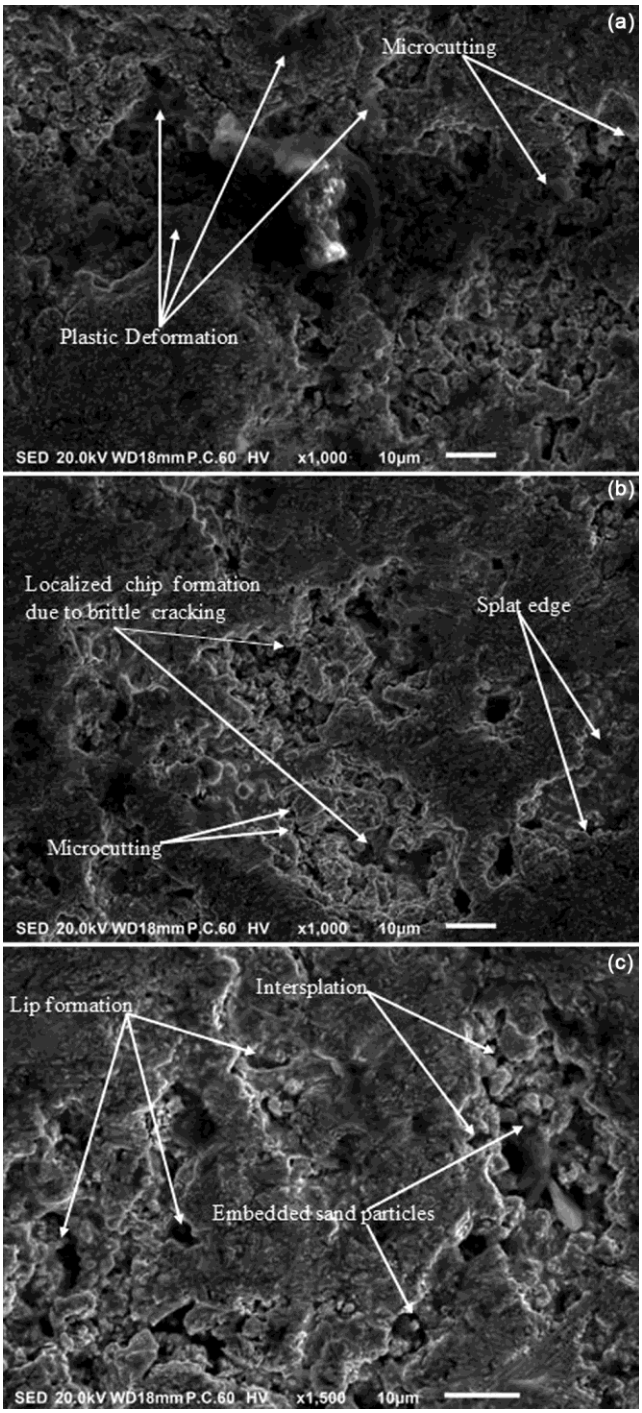

Fig. 24 — SEM images of HVOF-spray Cr_3C_2-NiCr coated steel post 120 mins of erosion testing at various impact angle (a) 30º, (b) 60º and (c) 90º.

suggests the displacement of the matrix due to plastic distortion inside the impact region. Hence, HVOF-spray Cr_3C_2–25NiCr coating exhibited a hybrid mode of erosion mechanism (i.e. ductile and brittle) with the brittle mode of erosion characteristic prevailing.

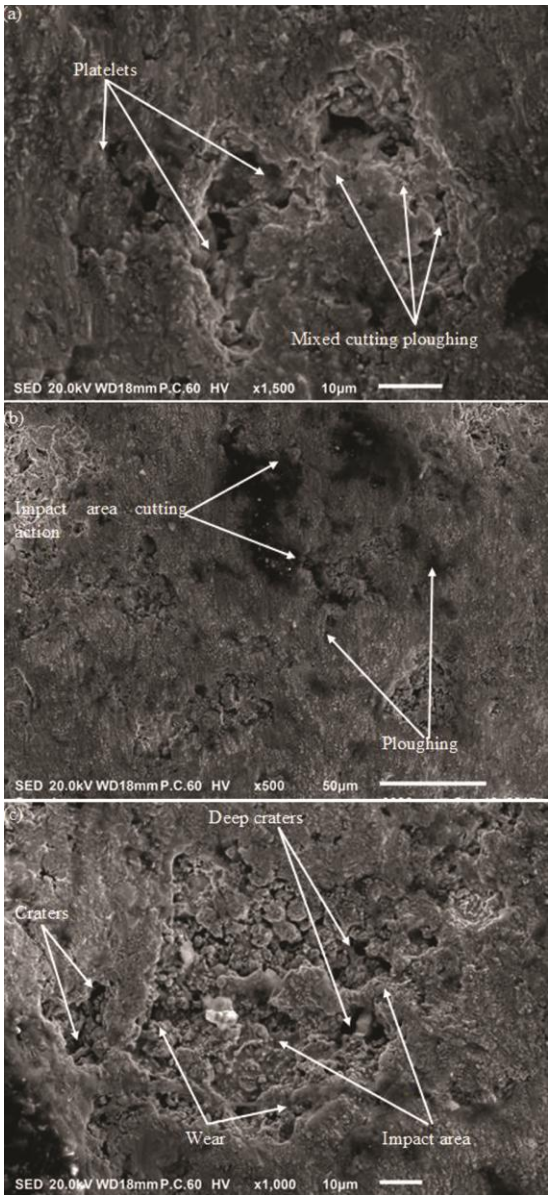

Fig. 25 — SEM images of HVOF-spray WC-10Co-4Cr coated steel post 120 mins erosion testing at various impact angles (a) 30º, (b) 60º and (c) 90º.

Further, it can be observed that under low velocity and low impact angle the main mechanism of degradation of the material was microchipping. Erodent particle's impact on the large-sized splat surface causes erosion in a fragile manner with localized chipping which extended to the splat boundaries. It has been found that observations are in line with the results of other researchers[25-26].

The results of erosion testing for HVOF-spray WC-10Co-4Cr coatings under slurry erosion conditions are shown in Fig. 25(a-c). It has been noticed that microchipping, ploughing, debonding and fracture

due to splat are major reasons for erosion. The removal of material from the surface is due to the lesser splat adhesive strength which resulted in the removal of entire splats. The impact of erodent particles fractured the coated surface and resulted in the propagation of cracks along the splat boundaries. The intersection of cracks resulted in the formation of chip material which gets ejected by the repetitive impact of particles like that of brittle materials[18, 22]. Fig. 25(a) illustrated the degradation mechanism of HVOF-spray WC-10Co-4Cr coating at impact angle 30º, impact velocity 25 m/s and slurry concentration 10000 ppm. It has been observed that erosion loss occurred due to the micro-cutting of a binder matrix followed by WC grains pull out. Further, it has been noticed that there is a presence of the short grooving which verified the fact that material removal has taken place due to the grooving mechanism. This grooving phenomenon further revealed the fact that binder material and WC grains were extruded simultaneously. In case of impact angle 90º, impact velocity 75 m/s and slurry concentration 30000 ppm, Fig. 25(b-c) depicts the presence of voids like feature which might be occurred due to WC pull out. It has been observed that the main wear mechanisms are fracturing and pull out of WC grains from the Co-Cr matrix. Furthermore, it was observed that the recurring strike of erodent particles on the target surface has made the metallic binder vulnerable owing to which pit formation takes place.

6 Conclusions

In this research paper, slurry erosion behaviour of uncoated steel, HVOF-spray Cr_3C_2-25NiCr and WC-10Co-4Cr coatings deposited on AISI304 steel were investigated in different slurry erosion conditions by changing impact velocity, impact angle and slurry concentration. The comparative analysis in terms of experimental results and microstructure was carried out among uncoated and coated AISI304 steel. From the analysis of the uncoated and coated steel following conclusions are drawn.

(i) The HVOF-spray Cr_3C_2-25NiCr and WC-10Co-4Cr coatings were observed to be effective in enhancing the slurry erosion resistance of AISI304 steel. It might be due to the higher hardness of the HVOF-spray coatings in comparison with AISI304 steel. Further, slurry erosion resistance of WC-10Co-4Cr coating was found to be higher than Cr_3C_2-25NiCr coatings. Hence, it can be concluded that the hardness of the target surface plays an important role in providing resistance against slurry erosion.

(ii) Among the three parameters, namely impact velocity, slurry concentration and impact angle, the impact velocity of slurry particles can be inferred to be the most influential parameter.

(iii) From the SEM images of degraded AISI304 steel, it was observed that crater and lip formation, plastic deformation, cutting and ploughing were found to be the main mechanism responsible for material degradation. Also, it has been observed that higher erosion has taken place at a narrow impact angle, i.e. 30°, in comparison with higher impact angle, i.e. 90°. Hence it can be concluded that AISI304 showed ductile behaviour under slurry erosion conditions.

(iv) The mechanism responsible for the degradation of surface in case of HVOF-spray WC-10Co-4Cr coating was micro craters along with plastic deformation whereas, in case of HVOF-spray Cr_3C_2-25NiCr coating, it was due to spalling, brittle fracture, micro-cutting and micro craters due to localized chip formation that results from the formation of brittle cracks. Penetrating erodent acts as a wedge to further enhance the effect of brittle crack.

(v) The regression equation was further modeled to predict the erosion rate of the HVOF-spray Cr_3C_2-25NiCr and WC-10Co-4Cr coatings. The results obtained from the modeled equations were found to be in good agreement with the experimental results.

Acknowledgement

The authors would like to thank I.K. Gujral Punjab Technical University, Kapurthala for valuable support and guidance.

References

1 Bajracharya T R, Joshi C B, Saini R P & Dahlhaug O G, *Wear*, 264 (2008) 177.
2 Chawla V, Sidhu B S, Puri D & Singh P, *J Aust Ceram Soc*, 44 (2008) 56.
3 Sidhu B S, Puri D & Prakash S, *J Mater Process Technol*, 159 (2005) 347.
4 Federici M, Cinzia M, Moscatelli A, Gialanella S & Straffelini G, *Wear*, 368-369 (2016) 326.
5 Lawrence P & Atkinson E, *Irrig Drain Syste*, 12 (1998) 371.
6 Santa J F, Espitia L A, Blanco J A, Romo S A & Toro A, *Wear*, 267 (2007) 160.

7 Goyal D K, Singh H, Kumar H & Sahni V, *J Tribol*, 136 (2014) 041602.
8 Goyal D K, Singh H, Kumar H & Sahni V, *J Therm Spray Technol*, 21 (2012) 838.
9 Bitter J G A, *Wear*, 6 (1963) 169.
10 Ramesh M R, Prakash S, Nath S K, Sapra P K & Venkataraman B, *Wear*, 269 (2010) 197.
11 Yuan J, Chunwei M, Yang S, Yu Z & Hua L, *Surf Coat Technol*, 285 (2016) 17.
12 Hong S, Yuping W, Wang Q, Ying G, Li G, Gao W, Wang B & Wenmin G, *Surf Coat Technol*, 225 (2013) 85.
13 Thakur L & Arora N, *Wear*, 303 (2013) 405.
14 Mahdipoor M S, Tarasi F, Moreau C, Dolatabadi A & Medra M, *Wear*, 330-331 (2015) 338.
15 Elkholy E, *Wear*, 84 (1983) 39.
16 Goyal D K, Singh H & Kumar H, *J Eng Tribol*, 21 (2012) 838.
17 Gupta R, Singh S N & Sehadri V, *Wear*, 184 (1995) 169.
18 Mahapatra S S & Patnaik A, *Mater Desi*, 30 (2009) 2791.
19 Hong S, Yuping W, Wang Q, Ying G, Li G, Gao W, Wang B & Wenmin G, *Surf Coat Technol*, 225 (2013) 85.
20 Levy A V & Chik P, *Wear*, 89 (1983) 151.
21 Santa J F, Baena J C &Toro A, *Wear*, 263 (2007) 258.
22 Lopez D, Congote J P, Cano J R, Toro A P & Tschiptschin A P, *Wear*, 259 (2005) 118.
23 Grewal H S, Arora H S, Agrawal A, Singh H & Mukerjee S, *Procedia Eng*, 68 (2013) 484.
24 Dong G & Zhang J Y, *J Mater Sci Eng*, 21 (2003) 307.
25 Praveen A S, Sarangan J & Suresh S, *Int J Refract Met*, 52 (2015) 209.
26 Stack M M, Zhou S & Newman R C, *Mater Sci Technol*, 12 (2013) 261.
27 Levy A V, *Solid Particle Erosion and Erosion-Corrosion of Materials*, (ASM International, USA), 1995.
28 Hawthorne H M, Arsenault B, Immarigeon J P, Legoux J G & Parameswaran V R, *Wear*, 225–229 (1999) 825.
29 Prasad B K, Jha A K, Modi O P & Yegneswaran A H, *Tribol Lett*, 17 (2004) 301.
30 Manisekaran T, Kamaraj M, Sharrif S M & Joshi S V, *J Mater Eng Perform*, 16 (2007) 567.
31 Singh M, Banerjee J, Patel P L & Tiwari H, *J Hydraul Eng*, 19 (2013) 1.
32 Okonkwo P C, Shakoor R A, Zagho M M & Mohamed A M A, *Metals*, 6 (2016) 1.